HEFAT2010
7th International Conference on Heat Transfer, Fluid Mechanics and Thermodynamics
19-21 July 2010
Antalya, Turkey

FIXED GRID NUMERICAL SIMULATION OF CONDUCTIVE-RADIATIVE HEAT TRANSFER WITH COMPLEX FIXED AND MOVING IMMERSED BOUNDARIES

Łapka P.* and Furmański P.
*Author for correspondence
Institute of Heat Engineering,
Warsaw University of Technology,
Nowowiejska St. 21/25, 00-665 Warsaw,
Poland,
E-mail: plapka@itc.pw.edu.pl, pfurm@itc.pw.edu.pl

ABSTRACT

In this paper the new numerical approach, which is based on the fixed grid front tracking method combined with the immersed boundary technique, was adopted for the two-dimensional conduction-radiation solidification process of semitransparent materials. The presented method enables accurate dealing with solidification processes of semitransparent materials which have different optical and thermophysical properties of solid and liquid phases as well as with absorption, emission and reflection of the thermal radiation at the solid-liquid interface without applying moving mesh methods. Therefore this method might be applied for simulations of Czochralski or Bridgman oxide crystals growth processes. The proposed numerical approach was examined by solving several simplified thermal radiation problems with complex fixed and moving boundaries (phase change problems) both in two-dimensional and axisymmetric spaces. For some of them the accuracy of obtained results was proved by comparing with reference works, other showed capabilities of the proposed method. For simplified solidification processes of semitransparent materials three configurations of optical properties, i.e., semitransparent solid phase and opaque liquid phase, opaque solid phase and semitransparent liquid phase, semitransparent both phases were considered. The interface between solid and liquid phases was treated to be opaque, absorbing, emitting and reflecting diffusely the thermal radiation. Influence of different optical parameters on temperature distribution in the solidified system and on solid-liquid interface shape were investigated. Results of the numerical simulations show that the presented numerical approach works well in this kind of problems and is promising for simulation of real solidification processes of semitransparent materials.

NOMENCLATURE

I	[W/m^2/sr]	Radiation intensity
K_a	[1/m]	Absorption coefficient
K_e	[1/m]	Extinction coefficient
K_s	[1/m]	Scattering coefficient
L_f	[J/kg]	Latent heat of melting
L	[m]	Dimension of computational domain
T, T_m	[K], [K]	Temperature, melting temperature
V	[m/s]	Interface velocity
c	[J/kg/K]	Specific heat
h	[W/m^2/K]	Convective heat transfer coefficient
k	[W/m/K]	Thermal conductivity
$\mathbf{n}$, n	[-],[-]	Normal vector, refraction index
$\mathbf{q}$	[W/m^2]	Density of heat flux
$\mathbf{s}$	[m]	Radiation direction vector
t	[s]	Time

Special characters

ε	[-]	Surface emissivity
ρ	[kg/m^3]	Density
σ	[W/m^2/K^4]	Stefan-Boltzmann constant
Φ	[-]	Scattering phase function
ω	[-]	Albedo
τ	[-]	Optical thickness
Ω	[sr]	Solid angle

Subscripts

i	Solid-liquid interface
s, l	Solid, liquid phase
z	Solid or liquid phase
w, ∞	Wall, surroundings

Subscripts

*	Non-dimensional

INTRODUCTION

The phase-change process of semitransparent materials is found in the nature as well as in several devices and manufacturing processes. Melting of ice by the solar radiation and solidification of water in presence of the sunlight are examples of a phase-change process of translucent materials

found in the nature. The most well known technical applications are glass and optical fibers manufacturing. Some translucent fluoride of alkali metals e.g.: lithium and potassium fluorides or eutectic mixture of lithium, magnesium and potassium fluorides are used as phase change materials in high temperature thermal energy storage systems which are elements of solar dynamic space power systems. Semitransparent single oxide crystals such as yttrium aluminium garnet or gadolinium gallium garnet, are commonly produced by Czochralski and Bridgman methods. During production of these single crystals, heat transfer mainly controlled by the thermal radiation exerts strong influence on crystals quality. It means that formation of both structural defects and non-homogeneities in crystals is affected by the solid-liquid interface shape and temperature distribution in the furnace. Therefore the numerical simulation of heat and mass transport is essential for development of these manufacturing processes, especially for semitransparent materials which have a melting point at a high temperature. Then experiments or observations are extremely difficult to carry out and highly expensive.

Analysis of solidification with internal radiation is a challenging task. The heat transfer process with phase change becomes additionally complicated by non-linear influence of the thermal radiation on temperature field. Radiation in semitransparent materials is a volumetric phenomenon i.e. emission, absorption and scattering of thermal radiation is present in the whole volume so that semitransparent materials behave differently than opaque ones. Nevertheless, the numerical simulation of the solidification process of semitransparent materials have been undertaken by many researches. Abrams and Viskanta [1] were first who analyzed one dimensional transient melting and solidification in translucent medium. Chan et al. [2] proposed one-dimensional model of internal melting or solidification of semitransparent pure materials, which accounts for isothermal two-phase region i.e. the mushy zone between liquid and solid zones. This model was validated by meteorological observations. Lately Łapka and Furmański [3] extended the earlier work of [2] and analyzed two-dimensional solidification of semitransparent pure materials and binary or eutectic alloys. Non-equilibrium planar solidification model for emitting, absorbing and isotropically scattering medium subjected to radiative and convective cooling was introduced by Yao et al. [4]. The simulation of a canister with semitransparent PCM used as element of high temperature thermal energy storage system was performed by Sokolov et al. [5]. In the case of numerical simulations of semitransparent oxide single crystal Bridgman growth processes Brandon and Derby [6] were the pioneers. The first global analysis of heat transfer in the Czochralski growth process of semitransparent crystals was carried out by Tsukada et al. [7]. Until now there are also several studies, which consider different aspects of the growth process of semitransparent single oxide crystal, e.g.: simulation of face formation as well as coupled heat flow and segregation in the Bridgman growth of oxide crystals [8] or simulation of specular reflection at crystal side in the Czochralski furnace [9].

The fixed grid front tracking method [10] and the immersed boundary technique [10, 11] are well known in heat transfer and computational fluid dynamics but until now were not used to simulate conjugated conductive-radiative heat transfer with moving immersed boundaries. The current work demonstrates that both these methods can be combined together enabling accurate simulation of the thermal radiation in solid and liquid phases with participating, moving and highly curved solid-liquid interface between them. The main objective of the paper was thus presentation of this new numerical approach but not physical modeling. Therefore, the convection in the melt, which plays an important role in real solidification processes, was neglected.

PROBLEM FORMULATION

The presented numerical model was implemented to two-dimensional rectangular enclosure filled with superheated, solidifying pure liquid. Only the conductive and the volumetric radiative heat transfer modes were considered at current stage of work. It was assumed that external walls of the computational domain might be opaque, emitting and reflecting diffusively the thermal radiation and simultaneously subjected to the external convective cooling by the surroundings or they may be adiabatic. The medium inside the domain was treated as gray, emitting, absorbing and anisotropically scattering the thermal radiation. Thermophysical and optical properties of the medium were assumed constant and fixed for a particular phase. For the moving interface cases the solidification process started when the bottom wall temperature was decreased below fixed melting temperature of the medium. The solid-liquid interface was assumed to be absorbing and diffusively reflecting the thermal radiation.

For the sake of brevity the governed equations are presented in the final dimensionless form. Therefore following non-dimensional quantities are first introduced: specific heat $c^*=c_l/c_s$, thermal conductivity $k^*=k_l/k_s$, refraction index $n^*=n_z/n_{ref}$, radiation intensity $I^*=I/(4n_{ref}^2\sigma T_m^4)$, absorption coefficient $K_a^*=K_{a,z}/K_{a,ref}$, extinction coefficient $K_e^*=K_{e,z}/K_{e,ref}$, scattering coefficient $K_s^*=K_{s,z}/K_{s,ref}$, heat flux $q^*=q/(4n_{ref}^2\sigma T_m^4)$, temperature $T^*=T/T_m$, velocity $V^*=Vc_s\rho_sL_x/k_s$, coordinates $x^*=x/L_x$ and $y^*=y/L_x$ (Cartesian 2D), $r^*=r/L_r$ and $z^*=z/L_r$ (axisymmetric), dimensions $L_{x^*}=L_x/L_x=1.0$ and $L_{y^*}=L_y/L_x$ or $L_{r^*}=L_r/L_r=1.0$ and $L_{z^*}=L_z/L_r$, density $\rho^*=\rho_l/\rho_s$, optical thickness $\tau=K_{e,ref}L_x$, albedo $\omega=K_{s,ref}/K_{e,ref}$, conduction-radiation parameter $N_r=k_s/(4n_{ref}^2\sigma T_m^3L_x)$, Fourier number $Fo=k_st/(c_s\rho_sL_x^2)$, Nusselt number $Nu=hL_x/k_s$ and Stefan number $Ste=c_sT_m/L_f$. Optical dimensionless parameters used in the presented study depend on the configuration between optical properties of the solid and liquid phases, i.e., when solid phase was semitransparent and liquid phase was opaque the RTE was solved only in solid phase, the liquid phase was blocked-off and it was assumed that $z=s$, $ref=s$. Similarly for other cases: when solid phase was opaque and liquid phase was semitransparent: $z=l$, $ref=l$, when both phases were semitransparent: $z=s$, $ref=l$. Farther details about mathematical formulation can be found in [12].

Considering the assumptions listed above and dimensionless parameters the non-dimensional transient energy equation (EE) for solid and liquid phase, respectively including the heat conduction and the internal thermal radiation can be written as:

$$\frac{\partial T^*}{\partial \mathrm{Fo}} = \nabla^{*2}T^* - \frac{1-\omega}{\mathrm{N_r}} n^* K_a^* \tau \left(T^{*4} - \int_{4\pi} I^* d\Omega \right) \qquad (1)$$

$$\rho^* c^* \frac{\partial T^*}{\partial \mathrm{Fo}} = \nabla^* k^* \nabla^* T^* - \frac{1-\omega}{\mathrm{N_r}} n^* K_a^* \tau \left(T^{*4} - \int_{4\pi} I^* d\Omega \right) \quad (2)$$

with convective and adiabatic boundary conditions for external walls in the form:

$$-\frac{\partial T^*}{\partial n_w^*} = \mathrm{Nu}\left(T_w^* - T_\infty^*\right) \text{ and } -\frac{\partial T^*}{\partial n_w^*} = 0 \text{ for the solid phase,}$$

$$-k^* \frac{\partial T^*}{\partial n_w^*} = \mathrm{Nu}\left(T_w^* - T_\infty^*\right) \text{and } -k^* \frac{\partial T^*}{\partial n_w^*} = 0 \text{ for the liqud phase.}$$

The radiative heat transfer in absorbing, emitting and scattering grey media along the line-of-sight s is described by the dimensionless radiative transfer equation (RTE):

$$\frac{1}{\tau}\frac{dI^*}{ds^*} = -K_e^* I^* + \frac{(1-\omega) n^* K_a^*}{4\pi} T^{*4} + \frac{\omega K_s^*}{4\pi} \int_{4\pi} I^* \Phi(\mathbf{s}' \to \mathbf{s}) d\Omega' \quad (3)$$

Terms present on the right hand side of RTE contribute to: attenuation of the radiation intensity by the absorption and out-scattering of the medium, augmentation of the radiation intensity by the self emission of the medium, augmentation of the intensity by the in-scattering from other directions, respectively. Assuming that walls of the domain and the solid-liquid interface were opaque, absorbing, emitting and reflecting diffusively the internal radiative boundary and interface conditions for the RTE, Eq. (3), for all outgoing directions ($\mathbf{s}^* \cdot \mathbf{n}^*_w > 0$) took the following form:

$$I^*_{w/i} = \frac{n^* \varepsilon_{w/i} T^{*4}_{w/i}}{4\pi} + \frac{1-\varepsilon_{w/i}}{\pi} \int_{\mathbf{s}^* \cdot \mathbf{n}^*_{w/i} < 0} I^* \left| \mathbf{s}^* \cdot \mathbf{n}^*_{w/i} \right| d\Omega . \quad (4)$$

The wall and the solid-liquid interface radiative heat fluxes were calculated from the formula:

$$q^*_{rw/i} = \int I^* \left| \mathbf{s}^* \cdot \mathbf{n}^*_{w/i} \right| d\Omega \quad (5)$$

with following conditions: $\mathbf{s}^* \cdot \mathbf{n}^*_{w/i} < 0$ for incident radiative flux (in) and $\mathbf{s}^* \cdot \mathbf{n}^*_{w/i} > 0$ for emitted radiative flux (out).

The local solid-liquid interface velocity was determined from the energy balance at the solid-liquid interface (Stefan condition) including incident radiative heat fluxes at the interface from the solid phase ($q^*_{ri,s,in}$) and liquid phase ($q^*_{ri,l,in}$) as well as emitted radiative heat fluxes at the interface into solid phase ($q^*_{ri,s,out}$) and liquid phase ($q^*_{ri,l,out}$):

$$V_i^* = \frac{\mathrm{Ste}}{\rho^*} \left(\left.\frac{\partial T^*}{\partial n^*}\right|_s - k^* \left.\frac{\partial T^*}{\partial n^*}\right|_l + \frac{q^*_{ri,s,out} + q^*_{ri,l,out} - q^*_{ri,s,in} - q^*_{ri,l,in}}{\mathrm{N_r}} \right) \quad (6)$$

In above equation incident and emitted radiative heat fluxes at the solid-liquid interface were calculated using Eq. (5) and the nearest nodal intensity values.

NUMERICAL METHOD

The non-dimensional EEs and RTE, Eqs. (1-3), were discretized using the Finite Volume Method (FVM) [13]. The computational domain was uniformly divided into a non-overlapping rectangular grid with a size dx in the x or r-axis direction and dy in the y or z-axis direction. Each term of the non-dimensional EEs was integrated over an interval of a dimensionless time $d\mathrm{Fo}$ and over a control volume dV. The dimensionless RTE was solved by the FVM for the radiative heat transfer [14]. The method was based on integration of the RTE over a control volume dV and over a control solid angle $d\Omega$. The same uniform, rectangular spatial grid as for the EEs was used. Additionally, in the FVM for the thermal radiation it is necessary to divide the whole solid angle into control solid angles. Therefore the whole azimuthal angle 2π and the whole polar angle π were divided uniformly into a non-overlapping angular grid with spacing $d\phi$ and $d\theta$, respectively, and the total number of control angles (discrete directions) was M. Discrete form of RHT for the axisymmetric geometry was derived from 3D formulation by applying special mapping procedure as explained in [15]. In such implementation the angular redistribution terms, which are found in RTE for cylindrical coordinates, were avoided.

Front Tracking Method

Solidification problem was solved by front tracking method [10]. In this method the non-dimensional governing equations, Eqs. (1-3), were solved implicitly on a fixed mesh and the interface was tracked explicitly. The solid-liquid interface was identified by an ordered set of mass-less marker points. A line connecting marker points represents the solid-liquid interface. If the distance between two marker points was larger than the assumed value the new marker point was placed between them. On the other hand if the distance between two marker points was smaller than the assumed value one of them was replaced or removed. Initially marker points were distributed uniformly over boundaries subjected to the external cooling. Marker points always advanced in a direction perpendicular to the solid-liquid interface at a growth velocity calculated form Eq. (6) and they had the temperature T^*_i. New positions of marker points were determined from their old positions, time interval and velocities:

$$x_i^{*new} = x_i^{*old} + d\mathrm{Fo} \cdot V_i^* \quad (7)$$

The marker velocity was calculated as follows. Temperature normal gradients into solid and liquid phase which appear in Eq. (6), were obtained by using the linear interpolation along the normal to the interface at point i as shown in Figure 1A. This approach was simple and convenient. Four points, two in the solid phase (n_1 and n_2) and two in the liquid phase (n_3 and n_4), which lie at the line normal to the interface at point i, were selected. The spacing between points i, n_1, n_2, and i, n_3, n_4 (Figure 1A) was fixed and equal to Δ. Then temperature values at these four points (n_1 to n_4) were obtained by the bilinear interpolation based on four nearest nodal values of temperatures. The gradient pointing into solid phase was then calculated from the expression:

$$\left.\frac{\partial T^*}{\partial n^*}\right|_s = \frac{4T^*_{n1} - T^*_{n2} - 3T^*_i}{2\Delta} \quad (8)$$

Similar expression was applied for the gradient pointing into liquid phase. Next, by using the Eq. (5) the incident ($q^*_{ri,s,in}$, $q^*_{ri,l,in}$) and emitted ($q^*_{ri,s,out}$, $q^*_{ri,l,out}$) radiative fluxes at the marker point i were calculated. To find these incident fluxes nodal intensity values of the control volume, at which boundary

marker point i lies, were used. Finally, the marker velocity was obtained from Eq. (6).

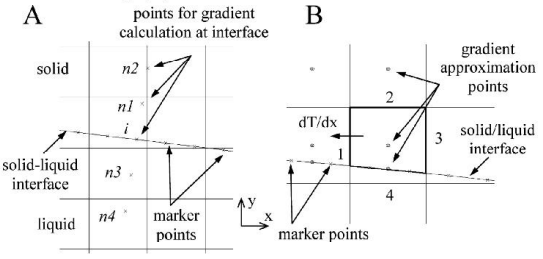

Figure 1. Scheme for interpolation: A - normal temperature gradients at interface, B - gradients at faces of trapezoidal cells.

Immersed Boundary Technique for Energy Equation

Calculations were performed on the fixed Cartesian grid. For the case when the rectangular mesh was cut by the solid-liquid interface the immersed boundary technique was applied [10]. This technique enables handling different optical and thermophysical properties of solid and liquid phases and phenomena that occur at the solid-liquid interface. This is different than in the case of the enthalpy method, which assumes average properties at control volumes that contain the solid-liquid interface, and therefore, is not suitable for dealing with opaque, absorbing, emitting and reflecting diffusively interface. In the immersed boundary technique these phenomena can be incorporated into calculations with ease. Also the refraction of radiation at the solid-liquid interface can be included. At first cells cut by the interface were selected and intersection points were found. Then the phase, in which cell center lied, was identified. By using special procedure new control volumes, which were in general trapezoidal in shape, were formed on both sides of the solid-liquid interface as shown in Figure 1B. Subsequently the finite volume discretization was applied to those irregular cells. Heat fluxes at faces no. 1 and 3 (see Figure 1B) were calculated using the two-dimensional interpolation function that was linear in the x or r-axis direction and quadratic in the y or z-axis direction:

$$T = c_1 xy^2 + c_2 y^2 + c_3 xy + c_4 y + c_5 x + c_6 \text{ for 2D} \qquad (9)$$

The x or r-component of temperature gradient was then directly determined by differentiation of Eq. (9):

$$\frac{\partial T}{\partial x} = c_1 y^2 + c_3 y + c_5 \text{ for 2D} \qquad (10)$$

Similar expression were constructed for gradients in the y or z-axis direction but the interpolation function was quadratic in the x or r-axis directions while linear in the y or z-axis direction. The temperature gradient at face no. 4 was calculated by using the linear interpolation along the normal to the interface – Eq. (8), while for the face 2 the standard finite volume approximation was adopted. Then Eq. (8) and Eq. (10) for gradients at trapezoidal control volume faces were incorporated into the global system of equations for temperature.

Immersed Boundary Technique for RTE

In case of immersed boundary method for RTE, the additional term which accounts for emission and reflection of radiation at the solid-liquid interface was incorporated into discrete form of RTE for Cartesian grid following Byun et al. [11]. Also the radiative fluxes i.e.: $q^*_{r,s,in}$, $q^*_{r,s,out}$, $q^*_{r,l,in}$, $q^*_{r,s,out}$ incoming and leaving the interface were calculated according to (Eq. 5) in order to find interface velocity from Eq. (6).

In the present paper it was assumed that the thermal radiation may propagate either in one phase: solid or liquid or in both phases. For the case when the thermal radiation was present only in one phase, the other one was blocked-off. The solid-liquid interface was assumed to be opaque, absorbing, emitting and reflecting diffusively, kept at fixed temperature T_i equal to the melting temperature T_m. But the presented numerical approach can also be implemented when the solid-liquid interface is semitransparent and is treated as the Fresnel interface. Then this numerical procedure should incorporate Snell's law at the solid-liquid interface and should be developed to conserve radiant energy transferred from one angular direction to another as a results of reflection and refraction of the thermal radiation at the solid-liquid interface.

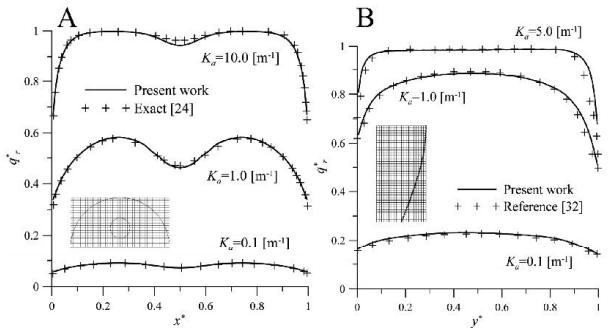

Figure 2. Comparison of dimensionless radiative heat fluxes distribution at the bottom wall of the two-dimensional semicircular enclosure with an internal circle (A) and at the right wall of the axisymmetric nozzle-shaped enclosure (B).

VERIFICATION OF THE NUMERICAL MODEL

Results obtained from the presented numerical model were compared with results of other studies. For the sake of brevity only few examples for the thermal radiation were presented. Details about numerical calculations setup were omitted but they can be found in the references. Numerical results for pure radiation problem for two-dimensional and axisymmetric geometry were compared with the results presented by Byun et al. [11] and by Salah et al. [16], respectively. In Figure 2A dimensionless radiative heat fluxes at the bottom wall of the two-dimensional semicircular enclosure with empty internal circle for different values of the absorption coefficients are presented against the exact results [11]. Comparison of the results of Salah et al. [16] for the axisymmetric nozzle-shaped enclosure with current work is shown in Figure 2B. All results are found to be in good agreement.

SIMULATION OF SOLIDIFICATION PROCESS

The proposed numerical model was subsequently applied to solve radiation-conduction dominated solidification process of semitransparent materials for two-dimensional and axisymmetric geometry to show capabilities and potential application area of the presented method. Influence of the conduction radiation parameter N_r on temperature fields and on the solid-liquid interface locations were also examined in order

to find an impact of the thermal radiation on phase change process. Calculations were performed assuming following configurations of the optical properties: (A) semitransparent solid phase and opaque liquid phase, (B) opaque solid phase and semitransparent liquid phase, (C) semitransparent both solid and liquid phases.

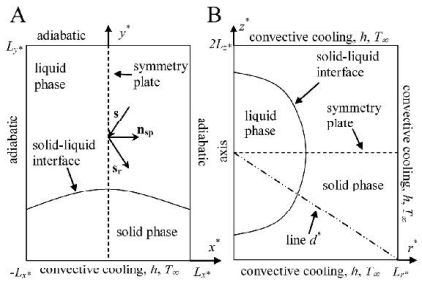

Figure 3. Schematic sketches of computational domains: (A) – two-dimensional and (B) – axisymmetric.

Two-dimensional Cartesian simulation

The two-dimensional rectangular enclosure with the width and the height equal to $2L_{x*}$ and L_{y*}, as shown in Figure 3A, was at the first investigated. It was assumed that the bottom boundary was opaque, emitting and reflecting diffusively and subjected to the external convective cooling by the surroundings. The other walls were treated as adiabatic. Most of thermophysical and optical properties of the medium were taken for YAG crystals. The dimensionless quantities were fixed at the following constant values: c^*=1.0, k^*=0.5, n^*=1.0, T^*_{init}=1.1, L_{x*}=1.0, L_{y*} =2.0, K_e^*=1.0, K_s^*=1.0, Fo=0.3, Nu=10^6, Ste=3.46, ε_w=1.0, ε_i=0.3, ρ^*=1.0. The scattering phase function was assumed isotropic. To make the problem two-dimensional the ambient temperature was assumed to vary according to the relation: T^*_∞=0.85-0.1cos(πx^*). The properties, which changed during the calculation, were made equal to: N_r=1.0, **0.1**, 0.01, τ=10.0, **1.0**, 0.01 (the bold values were taken as the default ones). The spatial domain and the solid angle were discretised as: N_xxN_y=20x40 and N_ϕxN_θ=8x4, respectively. Due to symmetry of the thermal problem a half of the medium in the cavity was considered.

In Figure 4 distributions of dimensionless temperature at x^*=0.5 and solid-liquid interface locations are shown as a function of the conduction-radiation parameter N_r. As N_r increases, the heat conduction becomes dominant. Semitransparent solid or liquid phase are then less radiatively cooled and eventually for N_r above unity solidification proceeds as for an opaque material. Decreasing N_r favors internal radiative cooling and limits the share of conductive heat transfer in the total heat flux. For semitransparent solid (Figures 4A and 4C) temperature distribution becomes concave as heat becomes more directly transmitted to the wall by the thermal radiation. More heat is removed from the vicinity of the solid-liquid interface and therefore the rate of solidification is increased. For semitransparent liquid phase the internal radiation decreases temperature in bulk liquid, more heat is transferred by the thermal radiation to the solid-liquid interface, and therefore, the rate of solidification is lower than for semitransparent solid phase.

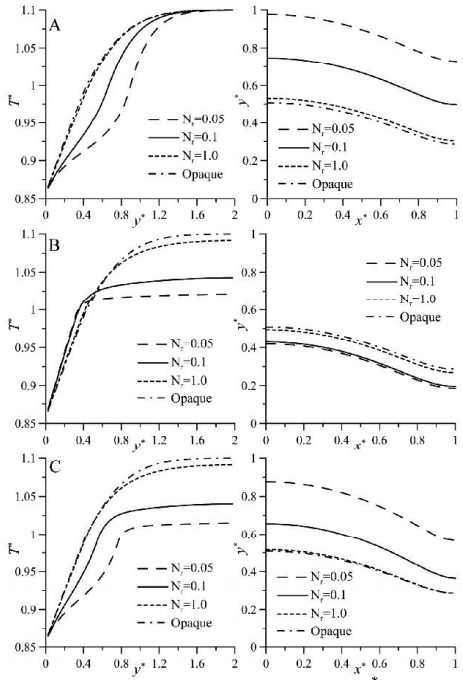

Figure 4. Temperature distributions along x^*=0.5 (left) and front locations (right) for varying N_r.

Axisymmetric simulation

The axisymmetric rectangular domain with the width and the height equal to L_{r*} and $2L_{z*}$, as shown in Figure 3B was also investigated. This geometry mimics a simplified metal canister used in the high temperature thermal energy storage system for the space applications. Right, top and bottom boundaries of the domain were subjected to external convective cooling by the surroundings, left wall was the axis of symmetry. Moreover, only a half of the medium in the cavity was considered due symmetry of the thermal problem. Most of thermophysical and optical properties of the medium were taken for fluoride salt with eutectic weight composition of LiF – 41.27%, MgF_2 – 48.76% and KF – 8.95%. The dimensionless quantities were fixed at the following constant values: c^*=1.0, k^*=1.0, n^*=1.0, ρ^*=1.0, T^*_{init}=1.1, T^*_∞=0.6, L_{r*}=1.0, L_{z*}=2.0, K_a^*=1.0, K_e^*=1.0, K_s^*=1.0, Fo=0.5583, Nu=1.1, Ste=1.69, ε_w=0.8, ε_i=0.6, ω=0.0. The scattering phase function was assumed isotropic The properties, which varied during the calculation, were made equal to: N_r=0.1, **0.2**, 0.42, τ=0.03, **0.3**, 3.0, 30.0. The spatial domain and the solid angle were discretised as: N_rxN_z=40x40 and N_ϕxN_θ=8x4, respectively.

In Figure 5 distributions of dimensionless temperature along line d^* (Figure 3B) and position of the solid-liquid interface are plotted for different optical configuration (cases A, B, C and opaque material). The internal radiation in liquid phase contributes to decreasing liquid temperature at the initial state of the process and to a little increase of solidification rate whereas internal radiation in solid phase increases heat transfer from the solid-liquid interface to the cooled boundaries and therefore strongly accelerates solidification. For the case A and C the solid-liquid interface propagates further than for case A

and opaque material. The thermal radiation effect is the most pronounced for the case C, and therefore, only results obtained for this case are further presented.

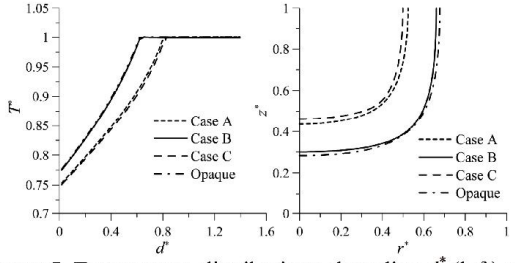

Figure 5. Temperature distributions along line d^* (left) and front locations (right) for different optical configurations.

The influence of the conduction-radiation parameter N_r for case C (semitransparent both solid and liquid phases) is shown in the Figure 6. The conclusion is the same as for Figure 6 – the share of the radiation in the total heat transfer increases as N_r falls and then radiative cooling through semitransparent solid is enhanced. Therefore more material is solidified as can be observed in Figure 6.

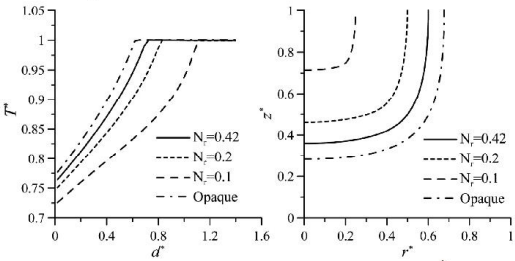

Figure 6. Temperature distributions along line d^* (left) and front locations (right) for varying N_r for case C.

CONCLUSIONS

In this work the front tracking method together with the immersed boundary technique was applied to solve solidification process of semitransparent materials. This combined approach enabled accurate dealing with different optical and thermophysical properties of solid and liquid phases as well as with the absorption, emission and reflection of the thermal radiation at the solid-liquid interface as was shown in the present paper. Moreover, being based on the fixed grid, the approach does not need adaptation of meshes to the solid-liquid interface shape and therefore, interpolation of field variables in every iteration of solving procedure seems unnecessary.

It was proved that the proposed method can be effectively used for solution of problems formulated in different coordinate systems. The numerical model was applied to two different geometrical configurations, i.e. two-dimensional Cartesian and axisymmetric cases with different thermophysical and optical properties in solid and liquid phases. The test cases with complex fixed boundaries reveal the good accuracy of the presented method, whereas simulation with complex moving boundaries and opaque, absorbing, emitting and reflecting diffusively solid-liquid interface show the capabilities and potential application area of the presented method.

Acknowledgments

This paper was partially financially supported by Polish Ministry of Science and Higher Education under Grant No. N N512 459736.

RFERENCES

[1] Abrams, M., and Viskanta, R., The Effect of Radiative Heat Transfer upon the Melting and Solidification of Semitransparent Crystals, *Journal of Heat Transfer*, vol. 96, 1974, pp. 184-190.

[2] Chan, S. H., Cho, D. H., and Kocamustafaogullari, G., Melting and Solidification with Internal Radiative Transfer – a Generalized Phase Change Model, *International Journal of Heat and Mass Transfer*, vol. 26, 1983, pp. 621-633.

[3] Łapka, P., and Furmański, P., Numerical Modeling of Solidification Processes of Semitransparent Materials Using the Enthalpy and the Finite Volume Methods, *Heat and Mass Transfer*, vol. 44, 2008, pp. 937-957.

[4] Yao, C., Wang, G.-X., and Chung, B. T. F., Nonequilibrium Planar Interface Model for Solidification of Semitransparent Radiating Materials, *Journal of Thermophysics and Heat Transfer*, vol. 14, 2000, pp. 297-304.

[5] Sokolov, P., Ibrahim, M., and Kerslake, T., Computational Heat-Transfer modeling of thermal energy storage canisters for space applications, *Journal of Spacecraft and Rockets*, vol. 37, 2000, pp. 265-272.

[6] Brandon, S., and Derby, J. J., Internal Radiative Transport in the Vertical Bridgman Growth of Semitransparent Crystals, *Journal of Crystal Growth*, vol. 110, 1991, pp. 481-500.

[7] Tsukada, T., Kakinoki, K., Hozawa, M., and Imaishi, N., Effect of Internal Radiation within Crystal and Melt on Czochralski Crystal Growth of Oxide, *International Journal of Heat and Mass Transfer*, vol. 38, 1995, pp. 2707-2714.

[8] Lan, C. W., and Tu, C. Y., Three-Dimensional Simulation of Facet Formation and the Coupled Heat and Segregation in Bridgman Growth of Oxide Crystals, *Journal of Crystal Growth*, vol. 233, 2001, pp. 523-536.

[9] Yuferev, V. S., Budenkova, O. N., Vasiliev, M., Rukolaine, S. A., Shlegel, V. N., Vasiliev, Ya. V., and Zhmakin, A. I., Variation of Solid-Liquid Interface in the BGO Low Thermal Gradients Cz Growth for Diffuse and Specular Crystal Side Surface, *Journal of Crystal Growth*, vol. 253, 2003, pp. 383-297.

[10] Ye, T., Mittal, R., Udaykumar, H. S., and Shyy, W., An Accurate Cartesian Grid Method for Viscous Incompressible Flow with Complex Immersed Boundaries, *Journal of Computational Physics*, vol. 156, 1999, pp. 209-240.

[11] Byun, Y. D., Baek, S. W., and Kim, M. Y., Investigation of Radiative Heat Transfer in Complex Geometries Using Blocked-Off, Multiblock, and Embedded Boundary Treatments, *Numerical Heat Transfer A*, vol. 43, 2003, pp. 807-825.

[12] Łapka, P., Furmański, P., Fixed grid simulation of radiation-conduction dominated solidification process, *Journal Heat Transfer*, vol. 132, 2010, pp. 023504-1-023504-10.

[13] Versteeg, H. K., and Malalasekera, W., An Introduction to Computational Fluid Dynamics. The Finite Volume Method, 2007, Pearson, Harlow, England.

[14] Raithby, G. D., and Chui, E., A Finite-Volume Method for Predicting a Radiant Heat Transfer in Enclosures with Participating Media, *Journal of Heat Transfer*, vol. 112, 1990, pp. 415-423.

[15] Murthy, J. Y., and Mathur, S. R., Radiative heat transfer in axisymmetric geometries using unstructured finite-volume method, *Numerical Heat Transfer B*, vol. 33, 1998, pp. 397-416.

[16] Salah, M. B., Askri, F., Jemni, A., and Nasrallah, S. B., Numerical Analyses of Radiative Heat Transfer in any Arbitrarily-Shaped Axisymmetric Enclosures, *Journal of Quantitative Spectroscopy and Radiative Transfer*, vol. 97, 2006,pp. 395–414.